arXiv:1611.01000v1 [cond-mat.mtrl-sci] 3 Nov 2016

Structure of twisted and buckled bilayer graphene

Sandeep K. Jain

Institute for Theoretical Physics, Universiteit Utrecht, Princetonplein 5, 3584 CC Utrecht, The Netherlands

E-mail: S.K.Jain@uu.nl

Vladimir Juričić

Nordita, Center for Quantum Materials, KTH Royal Institute of Technology and Stockholm University, Roslagstullsbacken 23, S-106 91 Stockholm, Sweden

Gerard T. Barkema

Department of Information and Computing Science, Universiteit Utrecht, Princetonplein 5, 3584 CC Utrecht, The Netherlands

Abstract. We study the atomic structure of twisted bilayer graphene, with very small mismatch angles ($\theta \sim 0.28^0$), a topic of intense recent interest. We use simulations, in which we combine a recently presented semi-empirical potential for single-layer graphene, with a new term for out-of-plane deformations, [Jain et al., J. Phys. Chem. C, 119, 2015] and an often-used interlayer potential [Kolmogorov et al., Phys. Rev. B, 71, 2005]. This combination of potentials is computationally cheap but accurate and precise at the same time, allowing us to study very large samples, which is necessary to reach very small mismatch angles in periodic samples. By performing large scale atomistic simulations, we show that the vortices appearing in the Moiré pattern in the twisted bilayer graphene samples converge to a constant size in the thermodynamic limit. Furthermore, the well known sinusoidal behavior of energy no longer persists once the misorientation angle becomes very small ($\theta < 1^0$). We also show that there is a significant buckling after the relaxation in the samples, with the buckling height proportional to the system size. These structural properties have direct consequences on the electronic and optical properties of bilayer graphene.

Keywords: Bilayer graphene, twist angle, Moiré pattern, empirical potential, local energy, vortices, buckling

1. INTRODUCTION

Bilayer graphene (BLG) consists of two stacked graphene sheets with usual stacking of either AB (Bernal) or AA type. However, two graphene layers can also be placed on top of each other in other arrangements, characterized in general by a mismatch angle θ. Such a structure is usually referred to as twisted bilayer graphene (TBLG)[1, 2], and represents an example of a Van der Waals heterostructure [3]. Since TBLG is made of two stacked misaligned lattices, a superlattice with a larger periodicity known as Moiré pattern emerges in the structure [4, 5].

Recently, this form of BLG has attracted a lot of attention theoretically and experimentally due to its exotic electronic [6, 7, 8, 9, 10, 11, 12, 13] and optical properties [14, 15, 16] arising due to the formation of the Moiré patterns. In particular, it has been theoretically suggested that the twist in the BLG may lead to a renormalization of the Fermi velocity [17], possible appearance of the flat electronic bands [18], neutrino-like oscillation of Dirac fermions [19] as well as localization of electrons [20]. Moreover, TBLG when placed in a magnetic field, exhibits a fractal spectrum of the Landau levels [21]. This theoretical interest has been motivated by the experimental observation of TBLG with Moiré patterns in the samples grown on SiC substrates[22], and using chemical vapour deposition [23, 24]. Furthermore, the mismatch angle has a significant impact on the quantum Hall effect in TBLG, as has been recently reported[25]; and breaking of the interlayer coherence for very small angles was experimentally found as well [26].

Out-of-plane buckling has a long-range effect in monolayer graphene and has significant impact on its structural properties and defect mechanics [27, 28, 29, 30, 31]. The resulting nanometer sized ripples have been studied experimentally by transmission electron microscopy (TEM) [32] and scanning probe microscopy [33, 34, 35, 36]. Recently, out-of-plane ripples in bilayer graphene have been detected and investigated via TEM [37, 38] and the combination of dark-field TEM with scanning transmission electron microscopy (STEM) [39]. The buckling effect in bilayer graphene has also been studied using computer simulations [40, 41, 42].

From the point of view of its electronic and structural properties, TBLG is most interesting when the mismatch angle is small. To theoretically obtain the structure of the TBLG with periodic boundary conditions and such small mismatch angles, it is necessary to consider samples with a large size. An approach based on an effective elastic potential is quite appealing in this regard since it allows to treat systems containing millions of atoms. Since we do not restrict ourselves to completely flat graphene layers but allow for some buckling, we use a combination of potentials, based on the recently developed semi-empirical potential for the monolayer graphene [31] with a new term describing out-of-plane deformations, and the more standard registry-dependent interlayer graphitic potential [43] to simulate relaxed large bilayer graphene structures with very small mismatch angle ($\theta \approx 0.28^\circ$). This combination of potentials is computationally cheap and accurate.

In energy-minimized (relaxed) samples, vortices arise in the atomic displacement field, due to the energy differences between different kinds of stacking, in agreement with previous studies [40, 42, 44]. We show that after relaxation the size of these vortices approaches a constant in the thermodynamic limit. Furthermore, we study out-of-plane buckling in bilayer graphene and find that the buckling height increases linearly with system size. We show that the buckling in the pristine bilayer graphene is significant (~ 3 Å) and forms a Moiré pattern analogous to the in-plane displacement without any singularities and with long range structural effects.

2. METHOD

We use a new combination of intra-layer and inter-layer potentials to simulate bilayer graphene. For the interactions within the same layer, we use the recently developed semi-empirical potential for single-layer graphene by Jain et al. [31], which has a new out-of-plane deformation term. The interlayer interactions are defined by the registry-dependent Kolmogorov-Crespi potential without the local normals [43]. This combination of empirical potentials is precise and accurate enough to capture the physical and structural changes in the system without any heavy computational requirements. These properties of the potential gives us freedom to study very large samples, which is required for having very small mismatch angles under periodic boundary conditions. In all samples studied, the energy is locally minimized, starting from well-informed choices for the initial configurations: insight obtained from many simulations of small systems is exploited to start the energy minimization of large samples from already well-relaxed samples. In our samples, we define a local energy per atom as follows: contributions due to two-body interactions are equally divided over the two interacting atoms, and contributions due to the three-body (angular) interactions are attributed to the central atom. Thus, the sum of the local energy over all atoms equals the total energy. This definition of local energy helps us to visualize the local degree of mechanical relaxation in the sample.

3. RESULTS AND DISCUSSION

We start with a sample having 1524 atoms in both layers with a mismatch angle of $\theta = 5.09^\circ$ between the layers as shown in Fig.1(a). The Moiré patterns are clearly visible in the sample along the diagonal. This sample is relaxed with the above described combination of potentials, and its effect on atomic relaxation in bottom and top layers is shown in Fig.1(b) and Fig.1(c), respectively. The arrows in the figure describe the relative atomic displacement after the relaxation with respect to the unrelaxed positions (i.e. the positions in top and bottom layer in the crystalline state of the individual graphene layers). Atoms near the center of AA stacking rotate to minimize the total energy and show a Moiré pattern of displacement vectors with respect to their initial positions in the form of vortices. In this case atoms in the bottom layer rotate in the

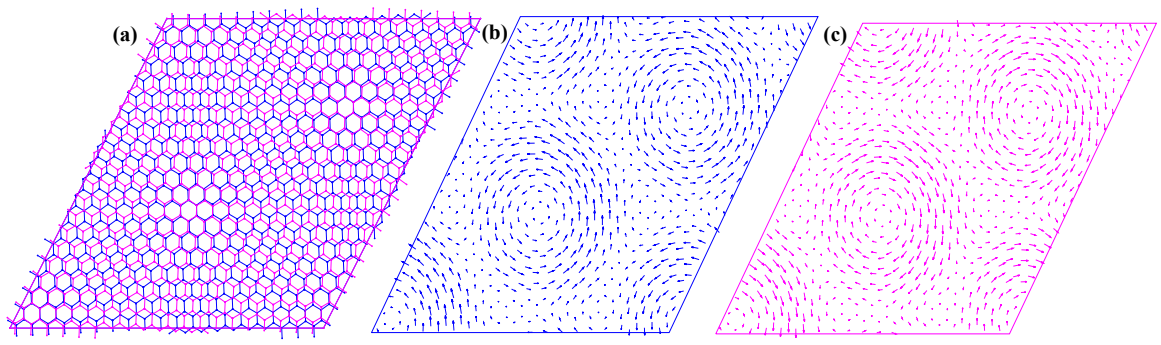

Figure 1: Bilayer graphene sample with 1524 atoms and with mismatch angle $\theta = 5.09°$. (a) Sample before relaxation. (b) Effect of relaxation in the bottom layer where atoms rotate counterclockwise near the vortex to minimize the total energy. (c) Effect of relaxation in the top layer where atoms rotate clockwise near the vortex in order to minimize the total energy. For visibility, the displacement arrows are enlarged by a factor of 20.

counterclockwise direction whereas atoms in top layer rotate clockwise, since the center of mass of the system is unaltered. During the process of relaxation the AA-stacked area becomes smaller while AB-stacked area grows, since the energy of AB-stacking is lower compared to AA-stacking. This result is in agreement with previous studies on TBLG [40, 44]. Relaxed bilayers have the intrinsic ripples in the structure and the equilibrium separation between the layers is 3.46 Å .

To study the effect of relaxation qualitatively, we generate a sample having 15132 atoms with a mismatch angle of 1.61°. The local energy profile of the sample before and after the relaxation is shown in Fig. 2(a) and Fig. 2(b), respectively. The binding energy of AA and AB stacking after the minimization is 11.8 meV/atom and 17.5 meV/atom respectively which is in very good agreement with reported values by Mostaani *et al.* calculated using quantum Monte Carlo technique [45]. The energy along the diagonal principal axis PQ behaves as a sinusoidal function before and after the relaxation for large values of the mismatch angle, as shown in Fig.2. However, this sinusoidal behaviour of energy is no longer present for small mismatch angles ($\theta < 1°$), as shown in Fig.3. The elastic energy becomes rather concentrated at the well-defined vortices in the displacement field. The local energy profile of the sample having 321,492 atoms with mismatch angle of 0.35°, before and after the relaxation is shown in Fig.3(a) and Fig.3(b), respectively. Our simulations show that before relaxation the size of the vortex around AA stacking increases linearly with system size $L \sim \sqrt{N} \sim 1/\theta$, with N as the number of atoms. The width of the peak at half maximum height along the diagonal PQ before the relaxation is given as W_{bv} and plotted as a function of $1/\theta$ in Fig.4(a). Here, the subscript b stands for 'before relaxation', and the subscript v for 'vortex'. Further on in this manuscript, we will also use subscripts a and l, which stand for 'after

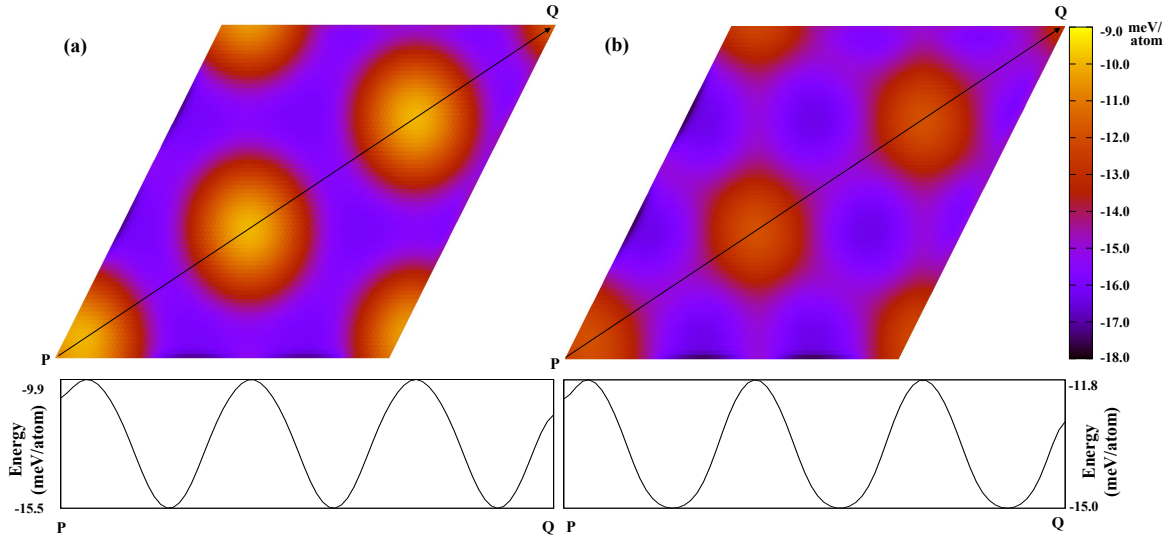

Figure 2: Local energy profile of a sample having 15132 atoms with $\theta = 1.61°$. (a) Before the relaxation. (b) After the relaxation. The bottom panel depicts the local energy along the main diagonal axis PQ which shows sinusoidal behaviour in this case.

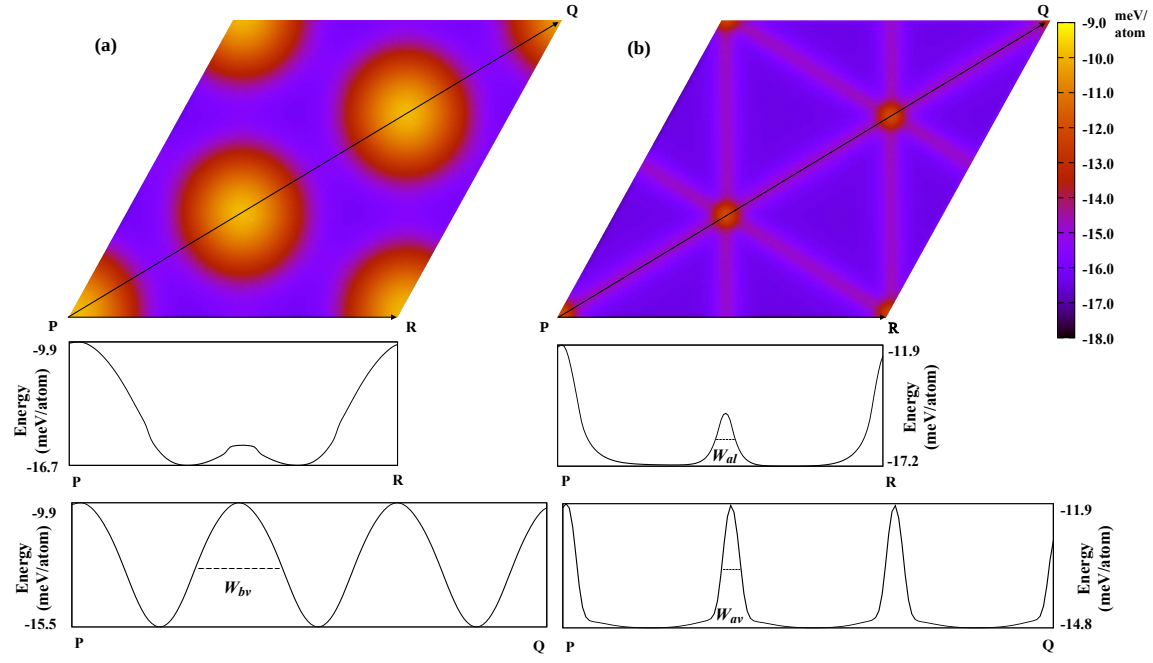

Figure 3: Local energy profile of a sample having 321,492 atoms with $\theta = 0.35°$. (a) Before the relaxation. (b) After the relaxation. The bottom panels depict the local energy along the two principal axes of the vortex lattice, horizontal PR and diagonal PQ. This shows that sinusoidal behaviour is not present at smaller θ along the PQ direction.

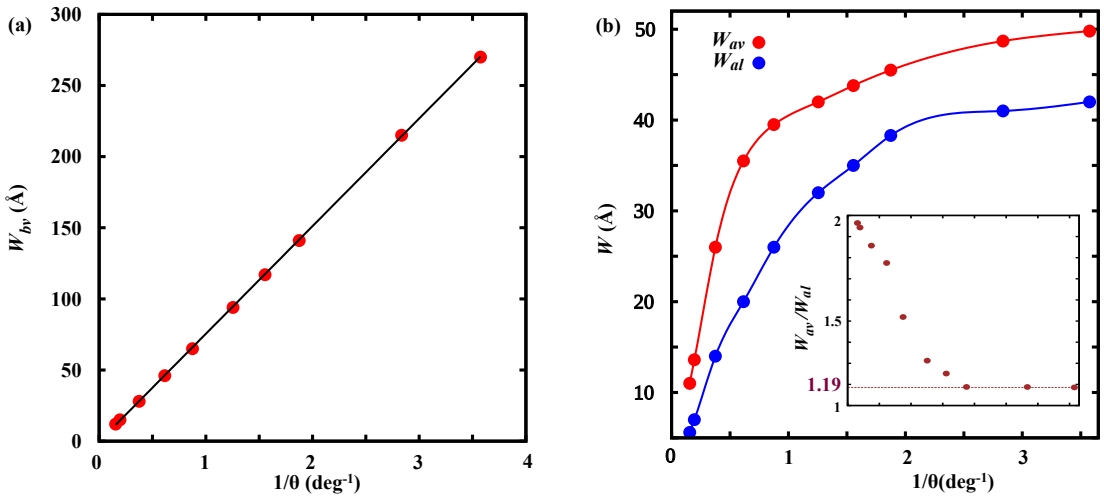

Figure 4: Scaling behaviour of peak widths corresponding to the size of the vortices as a function of inverse of the mismatch angle ($1/\theta$). We simulate the system sizes from 964 atoms ($\theta = 6.40°$) to 511,228 atoms ($\theta = 0.28°$). (a) W_{bv} (width of vortices peak at half its height, before relaxation) as a function of inverse of the mismatch angle. We observe a linear scaling with $1/\theta$. Since θ scales as inverse of L, W_{bv} scales linearly with system size. (b) W_{av} (width of vortices peak at half its height, after relaxation) and W_{al} (width of line peak at half its height, after relaxation) as a function of inverse of the mismatch angle. At large small mismatch angle ($\theta < 0.6°$) the ratio between these two peak widths becomes constant (inset).

relaxation' and 'line', respectively. We calculate the peak width along the diagonal PQ after the minimization (W_{av}) and plot it as a function of $1/\theta$ as shown in Fig.4(b). For large system size W_{av} appears to approach a constant value of ~ 50 Å . We also calculate the peak width after the minimization along the line PR, represented as W_{al}. In the local energy profile of relaxed samples, vortices are connected via a line which denotes a configuration with the structure in-between AA and AB stacking as shown in Fig.5(b). The binding energy of this kind of stacking is 14.8 meV. We plot W_{al} as a function of $1/\theta$ and find that at small mismatch angles (large system sizes) it also approaches a constant value of ~ 42 Å . The ratio between W_{av} and W_{al} becomes constant for all the systems with mismatch angle below 0.6° as shown in inset of Fig.4(b). We find that the value for the constant ratio is 1.19 in the thermodynamic limit.

The Bernal stacking in BLG has been investigated experimentally via STEM, where it has been shown that regions of AB and BA stacking are separated by nanometer wide rippled boundaries [37, 39]. In our simulations this is also the case as shown in Fig.3 where lines connecting the vortices are separating AB and BA stackings. We present the detailed structures of these vortices, lines and Bernal stackings with displacement fields in Fig.5. Recent studies by Dai *et. al.* determining the size of the lines and

vortices using the Peierls-Nabarro model [41, 42] are in very good agreement (within 10%) with our estimate of constant size in the thermodynamic limit. Alden *et. al.* use the Frenkel-Kontorava model [46] and report a size which is significantly larger than experimental observation [37].

With very small mismatch angles and thus very large Moiré patterns, most of the additional energy, ΔE, due to the Moiré pattern comes from the lines connecting the vortices, as these lines grow with decreasing angle, while the vortices do not. The additional energy due to the Moiré pattern is a combination of intralayer and interlayer energy terms. The intralayer energy contribution decreases inversely proportional to the line width w_{al}, while the interlayer energy contribution increases linearly with line width

$$\Delta E = a w_{al} L + b \frac{L}{w_{al}}, \tag{1}$$

where the parameter a is determined by the energy difference between the different stackings, and b is determined by the bulk modulus of a graphene layer.

In classical elastic bead spring models with a fixed extension, the extension per spring in the system decreases linearly with the number of the springs. With harmonic springs, the energy per spring scales quadratically with extension, and the total energy thus decreases linearly with the number of springs. Here in equation (1), w_{al} is analogous to the number of the springs. Therefore, the intralayer energy contribution decreases inversely proportional to the line width w_{al}. The interlayer energy simply depends on the mismatched area in the sample and therefore scales linearly with w_{al}.

Minimizing ΔE with respect to the line width results in an $L-$independent w_{al} given as

$$w_{al} = \sqrt{b/a}. \tag{2}$$

Therefore, in the large samples where the size of vortices becomes constant, the width of the line connecting the vortices also becomes constant since it only depends on the bulk modulus of graphene and the type of stacking between two layers. In our numerical simulations we find the trend which is consistent with this analytical argument. We have calculated the value of interlayer energy constant as $a = 0.0018$ eV/Å^2 and intralayer energy constant as $b = 3.1750$ eV by fitting our numerical energy data to equation (1).

We minimize the samples in all directions for two different boundary conditions: deformation-free (DF) boundary conditions where the periodic box is determined by the crystalline structure of single undeformed graphene layers, and force-free (FF) boundary conditions where changes in the simulation box are allowed [47]: the length of each of the periodicity vectors as well as the angle between them is determined by the constraint of minimal total energy. Our results on energetics of TBLG (Figs. 2-5) are based on DF boundary conditions since structures with DF boundaries allow us to compare atomic coordinates before and after relaxation without complications due to differences in box size. Moreover, we verified that the shrinkage in the box size and the differences in the energies between two different boundary conditions are very small ($< 0.08\%$) and do

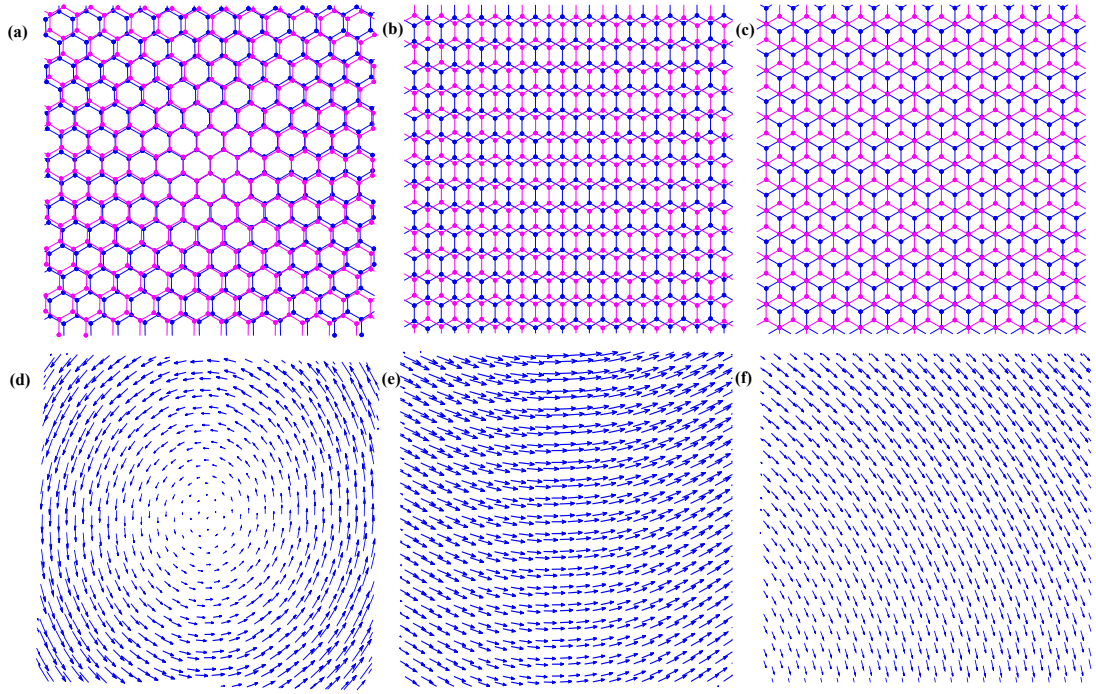

Figure 5: Detailed structures and displacement fields around a vortex, line and Bernal stacked (AB/BA) region. (a-c) Atomic structures of a vortex, line and Bernal stacked (AB/BA) region, respectively. Here blue color is used for bottom layer and magenta color is used for top layer. (d-f) Displacement fields around a vortex, line and Bernel stacked (AB/BA) region in bottom layer with respect to their unrelaxed positions, respectively.

not alter the results and predictions presented in the paper. But this small decrease in the box size has very significant consequences on the buckling height, which we discuss next.

We now consider out-of-plane deformations in the TBLG samples. Our samples before the relaxation have completely flat layers separated by 3.4 Å in the z-direction. The minimized structures have out-of-plane deformations characterized by the type of stacking between the layers. In Fig. 6(a) we show the structure of ripples in a sample with $N = 15132$ atoms after the complete relaxation. The equilibrium average separation distance is 3.44 Å in between the layers. The profile of out-of-plane deformations in the top layer is shown in Fig.6(b). The buckling height in the individual layer is 0.51 Å for DF boundaries. For FF boundaries the buckling height is more significant and reaches a value of 1.12 Å . The out-of-plane deformations along the diagonal PQ direction are plotted in both top and bottom layer, as shown in Fig.6(c). The behaviour along the PQ direction is sinusoidal and the separation around AA stacking is 3.62 Å , in good agreement with previously reported values in literature calculated using density functional theory (DFT) calculations [44, 48]. Most importantly, we observe a Moiré

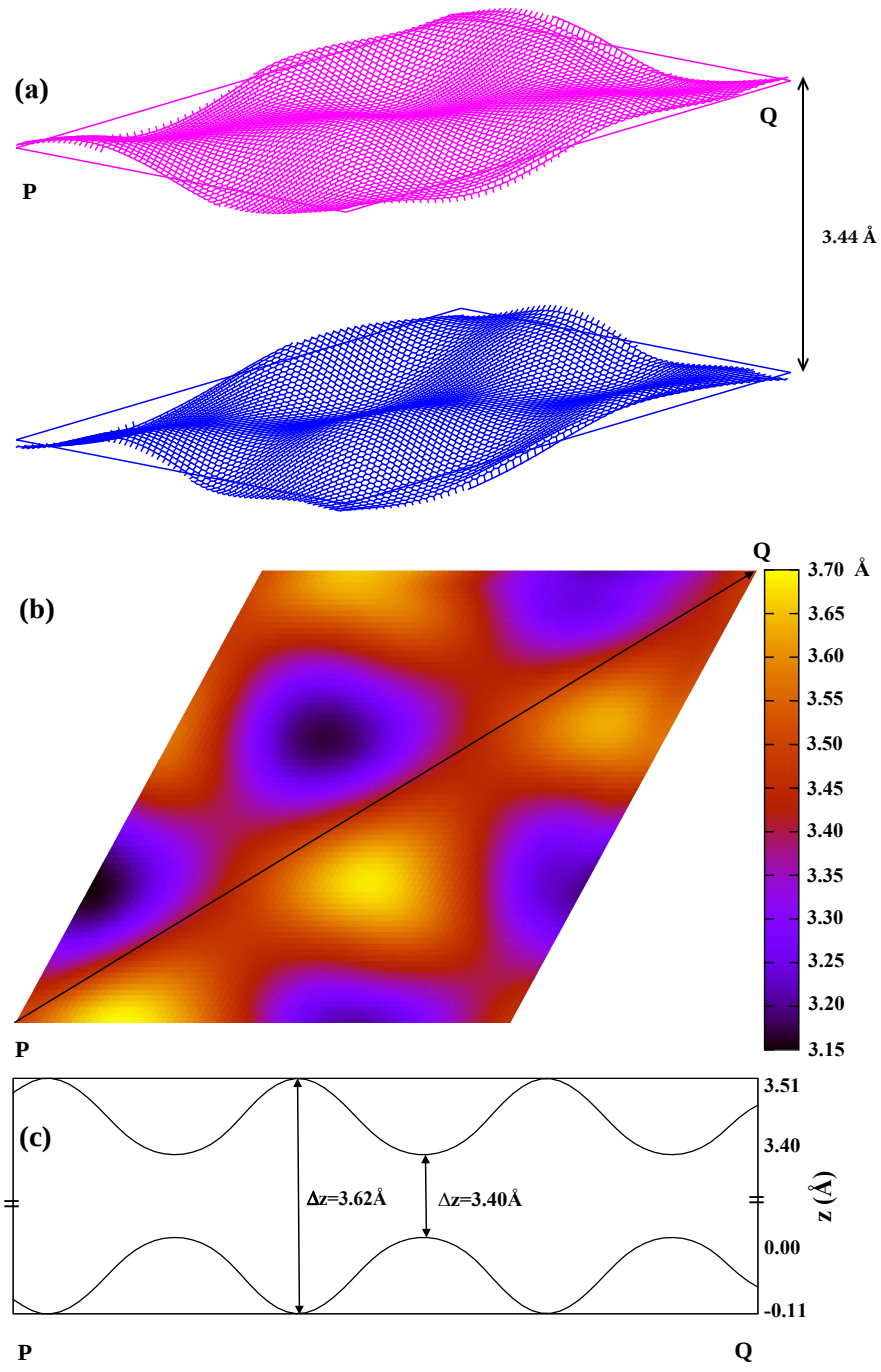

Figure 6: Buckling behaviour in a sample with 15132 atoms ($\theta = 1.61°$). (a) Ripples in both top and bottom layer. The equilibrium separation between both layers is 3.44Å . (b) Buckling profile of the top layer for DF boundary conditions. The buckling height is 0.51Å . (c) Buckling along the diagonal PQ in both the layers. Around the AA stacked area the separation between the layers is 3.62Å .

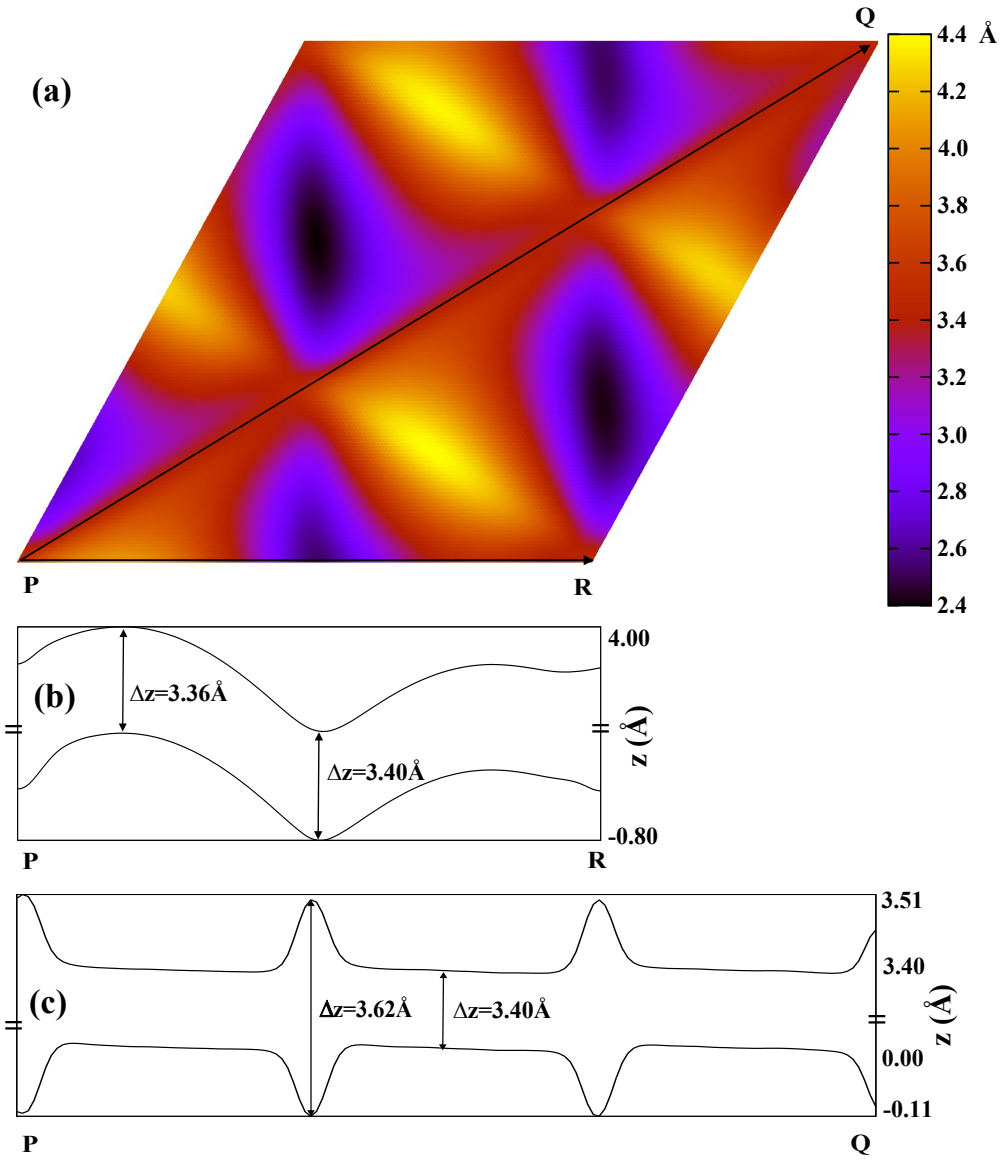

Figure 7: Buckling behaviour in a sample with 321,492 atoms ($\theta = 0.35°$). (a) Buckling profile of the top layer. The buckling height is 1.74Å . (b) Buckling along the line PR in both the layers. Around the AB stacked area the separation between the layers is 3.36Å . (c) Buckling along the diagonal PQ in both the layers. Around the AA stacked area the separation between the layers is 3.62Å . The equilibrium separation between both layers is 3.38Å .

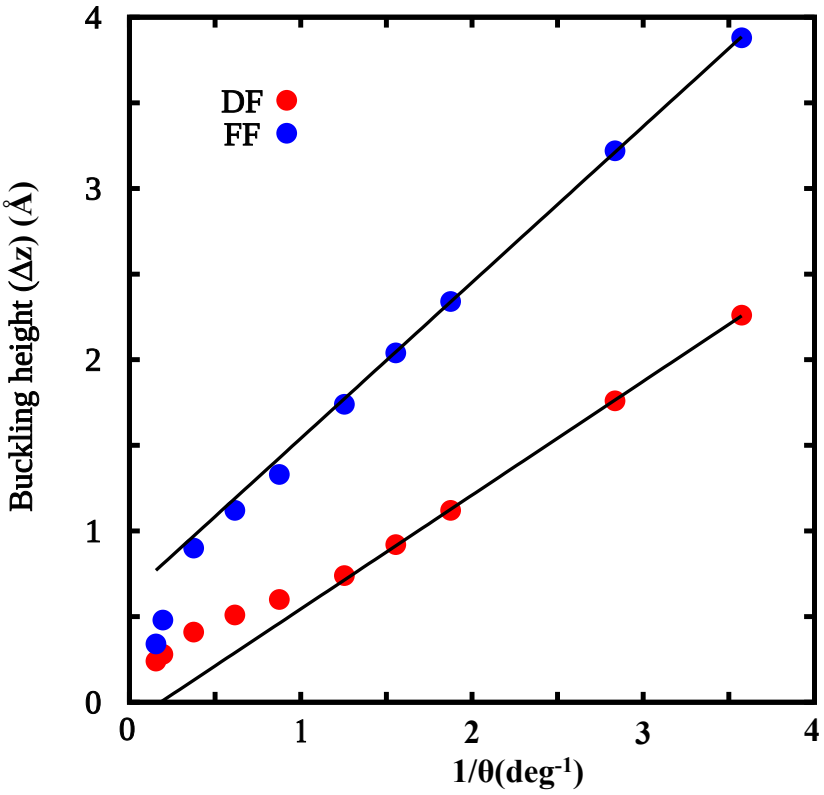

Figure 8: Buckling height as a function of inverse of the mismatch angle ($1/\theta$) for both DF and FF boundary conditions. For large system sizes (small θ),the scaling of the buckling height is linear with the system size. Intrinsic ripples are significant and have the values of height 2.3Å and 3.8Å for DF and FF boundary conditions, respectively, in a sample with $N = 511,228$ atoms with $\theta = 0.28°$.

pattern-like feature in the buckling height, see Figs.6(b) and 7(a).

We now discuss in more detail features of the spatial pattern in the buckling height. As we already pointed out, with increasing system size the vortex in the in-plane displacement around AA stacking shrinks after the minimization and appears to become constant for $\theta < 0.6°$. This feature yielding a characteristic length scale can also be seen in the buckling of a sample having 321,492 atoms ($\theta = 0.35°$), as shown in Fig.7. Namely, the characteristic length scale in this case is the equilibrium average separation distance, and its size relative to the system size decreases with increasing system size, since the AB stacked area grows and AA stacked area does not. In this case it has the value of 3.38 Å . The sinusoidal behaviour in the buckling, as shown in Figs.6(c), disappears for small mismatch angles as shown in Figs.7(c) . Finally, the buckling height increases linearly with system size for both DF and FF boundary conditions, as shown in Fig.8. The buckling height for the largest sample ($N = 511,228$ atoms with $\theta = 0.28°$) studied by our simulations for FF boundary conditions is quite significant as the value is 3.78 Å .

For the smallest twist angle under periodic boundary conditions ($\theta \sim 1/L \sim 1/\sqrt{N}$), each mismatch line seems to induce a small, constant buckling angle, which causes a buckling height that increases linearly with system size L. Without periodic boundaries, the twist angle is not discretized and can approach zero at any fixed system size; but we only simulated periodic boundaries. It is however clear that if at fixed L the twist angle approaches zero, the buckling height has to approach zero as well, as the system then gradually approaches the perfectly aligned crystal, which is flat.

4. CONCLUSIONS

Our work demonstrates the crucial importance of having large, well-relaxed samples of twisted bilayer graphene, to study its structural properties. The new combination of intralayer and interlayer potentials uses explicit lists of bonds and is therefore computationally very cheap. This allows us to accurately simulate very large TBLG samples with very small mismatch angles. The simulation results are in very good agreement with reported in the literature. There are sinusoidal modulations in the energy and buckling height for large misorientation angles but this behaviour no longer persists at small misorientation angles. We have shown with large scale atomistic simulations that the size of the vortices in the displacement field approaches a constant in the thermodynamic limit. There are significant out-of-plane deformations which increase with increasing system size. The characteristic average separation between the layers also becomes constant in the thermodynamic limit. These structural properties should have direct effect on electronic and optical properties of twisted bilayer graphene. In future work, the same combination of potentials can be modified with different structural parameters to investigate other misalinged two-dimensional materials such as h-BN, MoS_2 and WSe_2.

Acknowledgments

This project is funded by FOM-SHELL-CSER programme (12CSER049). This work is part of the research programme of the Foundation for Fundamental Research on Matter (FOM), which is part of the Netherlands Organisation for Scientific Research (NWO).

References

[1] Ohta T, Bostwick A, Seyller T, Horn K and Rotenberg E 2006 *Science* **313** 951–954 ISSN 1095-9203 URL `http://dx.doi.org/10.1126/science.1130681`

[2] Reina A, Jia X, Ho J, Nezich D, Son H, Bulovic V, Dresselhaus M S and Kong J 2009 *Nano Lett.* **9** 30–35 ISSN 1530-6992 URL `http://dx.doi.org/10.1021/nl801827v`

[3] Geim A K and Grigorieva I V 2013 *Nature* **499** 419–425 ISSN 1476-4687 URL `http://dx.doi.org/10.1038/nature12385`

[4] Lu C C, Lin Y C, Liu Z, Yeh C H, Suenaga K and Chiu P W 2013 *ACS Nano* **7** 2587–2594 ISSN 1936-086X URL `http://dx.doi.org/10.1021/nn3059828`

[5] Woods C R, Britnell L, Eckmann A, Ma R S, Lu J C, Guo H M, Lin X, Yu G L, Cao Y, Gorbachev R V and et al 2014 *Nat. Phys.* **10** 451–456 ISSN 1745-2481 URL http://dx.doi.org/10.1038/NPHYS2954

[6] Mele E J 2010 *Phys. Rev. B* **81** 161405 ISSN 1550-235X URL http://dx.doi.org/10.1103/PhysRevB.81.161405

[7] Lopes de Santos J M B, Peres N M R and Castro Neto A H 2007 *Phys. Rev. Lett.* **99** 256802 ISSN 1079-7114 URL http://dx.doi.org/10.1103/PhysRevLett.99.256802

[8] Shallcross S, Sharma S and Pankratov O A 2008 *Phys. Rev. Lett.* **101** 056803 ISSN 1079-7114 URL http://dx.doi.org/10.1103/PhysRevLett.101.056803

[9] de Gail R, Goerbig M O, Guinea F, Montambaux G and Castro Neto A H 2011 *Phys. Rev. B* **84** 045436 ISSN 1550-235X URL http://dx.doi.org/10.1103/PhysRevB.84.045436

[10] Bistritzer R and MacDonald A H 2011 *Phys. Rev. B* **84** 035440 ISSN 1550-235X URL http://dx.doi.org/10.1103/PhysRevB.84.035440

[11] Suarez Morell E, Vargas P, Chico L and Brey L 2011 *Phys. Rev. B* **84** 195421 ISSN 1550-235X URL http://dx.doi.org/10.1103/PhysRevB.84.195421

[12] Chae D H, Zhang D, Huang X and von Klitzing K 2012 *Nano Lett.* **12** 3905–3908 ISSN 1530-6992 URL http://dx.doi.org/10.1021/nl300569m

[13] Pelc M, Morell E S, Brey L and Chico L 2015 *The Journal of Physical Chemistry C* **119** 10076–10084 ISSN 1932-7455 URL http://dx.doi.org/10.1021/acs.jpcc.5b00685

[14] Moon P and Koshino M 2013 *Phys. Rev. B* **87** 205404 ISSN 1550-235X URL http://dx.doi.org/10.1103/PhysRevB.87.205404

[15] Tabert C J and Nicol E J 2013 *Phys. Rev. B* **87** 121402 ISSN 1550-235X URL http://dx.doi.org/10.1103/PhysRevB.87.121402

[16] De Corato M, Cocchi C, Prezzi D, Caldas M J, Molinari E and Ruini A 2014 *The Journal of Phys. Chem. C* **118** 23219–23225 ISSN 1932-7455 URL http://dx.doi.org/10.1021/jp504222m

[17] Yin L J, Qiao J B, Wang W X, Zuo W J, Yan W, Xu R, Dou R F, Nie J C and He L 2015 *Phys. Rev. B* **92** ISSN 1550-235X URL http://dx.doi.org/10.1103/PhysRevB.92.201408

[18] Suarez Morell E, Correa J D, Vargas P, Pacheco M and Barticevic Z 2010 *Phys. Rev. B* **82** 121407(R) ISSN 1550-235X URL http://dx.doi.org/10.1103/PhysRevB.82.121407

[19] Xian L, Wang Z F and Chou M Y 2013 *Nano Lett.* **13** 5159–5164 ISSN 1530-6992 URL http://dx.doi.org/10.1021/nl4024403

[20] Trambly de Laissardiere G, Mayou D and Magaud L 2010 *Nano Lett.* **10** 804–808 ISSN 1530-6992 URL http://dx.doi.org/10.1021/nl902948m

[21] Wang Z F, Liu F and Chou M Y 2012 *Nano Lett.* **12** 3833–3838 ISSN 1530-6992 URL http://dx.doi.org/10.1021/nl301794t

[22] Hass J, Varchon F, Milln-Otoya J E, Sprinkle M, Sharma N, de Heer W A, Berger C, First P N, Magaud L and Conrad E H 2008 *Phys. Rev. Lett.* **100** 125504 ISSN 1079-7114 URL http://dx.doi.org/10.1103/PhysRevLett.100.125504

[23] Luican A, Li G, Reina A, Kong J, Nair R R, Novoselov K S, Geim A K and Andrei E Y 2011 *Phys. Rev. Lett.* **106** 126802 ISSN 1079-7114 URL http://dx.doi.org/10.1103/PhysRevLett.106.126802

[24] Liu J B, Li P J, Chen Y F, Wang Z G, Qi F, He J R, Zheng B J, Zhou J H, Zhang W L, Gu L and et al 2015 *Sci. Reports* **5** 15285 ISSN 2045-2322 URL http://dx.doi.org/10.1038/srep15285

[25] Lee D S, Riedl C, Beringer T, Castro Neto A H, von Klitzing K, Starke U and Smet J H 2011 *Phys. Rev. Lett.* **107** 216602 ISSN 1079-7114 URL http://dx.doi.org/10.1103/PhysRevLett.107.216602

[26] Kim Y, Yun H, Nam S G, Son M, Lee D S, Kim D C, Seo S, Choi H C, Lee H J, Lee S W and et al 2013 *Phys. Rev. Lett.* **110** 096602 ISSN 1079-7114 URL http://dx.doi.org/10.1103/PhysRevLett.110.096602

[27] Fasolino A, Los J H and Katsnelson M I 2007 *Nat. Mat.* **6** 858 – 861

[28] Katsnelson M and Geim A 2008 *Phil. Trans. R. Soc. A* **366** 195–204

[29] Ma J, Alfè D, Michaelides A and Wang E 2009 *Phys. Rev. B* **80**(3) 033407 URL http://link.aps.org/doi/10.1103/PhysRevB.80.033407

[30] Chen S and Chrzan D C 2011 *Phys. Rev. B* **84**(21) 214103 URL http://link.aps.org/doi/10.1103/PhysRevB.84.214103

[31] Jain S K, Barkema G T, Mousseau N, Fang C M and van Huis M A 2015 *The Journal of Physical Chemistry C* **119** 9646 ISSN 1932-7455 URL http://dx.doi.org/10.1021/acs.jpcc.5b01905

[32] Meyer J C, Geim A K, Katsnelson M I, Novoselov K S, Booth T J and Roth S 2007 *Nature* **446** 60–63

[33] Ishigami M, Chen J H, Cullen W G, Fuhrer M S and Williams E D 2007 *Nano Letter* **7** 1643–1648

[34] Stolyarova E, Rim K T, Ryu S, Maultzsch J, Kim P, Brus L E, Heinz T F, Hybertsen M S and Flynn G W 2007 *Proceedings of the National Academy of Sciences* **104** 9209–9212 (*Preprint* http://www.pnas.org/content/104/22/9209.full.pdf) URL http://www.pnas.org/content/104/22/9209.abstract

[35] Capasso A, Placidi E, Zhan H, Perfetto E, Bell J, Gu Y and Motta N 2014 *Carbon* **68** 330 – 336 ISSN 0008-6223 URL http://www.sciencedirect.com/science/article/pii/S0008622313010579

[36] Ackerman M L, Kumar P, Neek-Amal M, Thibado P M, Peeters F M and Singh S 2016 *Phys. Rev. Lett.* **117**(12) 126801 URL http://link.aps.org/doi/10.1103/PhysRevLett.117.126801

[37] Butz B, Dolle C, Niekiel F, Weber K, Waldmann D, Weber H B, Meyer B and Spiecker E 2014 *Nature* **505** 533–537

[38] Meyer J, Geim A, Katsnelson M, Novoselov K, Obergfell D, Roth S, Girit C and Zettl A 2007 *Solid State Communications* **143** 101 – 109 ISSN 0038-1098 exploring grapheneRecent research advances URL http://www.sciencedirect.com/science/article/pii/S003810980700316X

[39] Lin J, Fang W, Zhou W, Lupini A R, Idrobo J C, Kong J, Pennycook S J and Pantelides S T 2013 *Nano Letters* **13** 3262–3268

[40] Wijk M M v, Schuring A, Katsnelson M I and Fasolino A 2015 *2D Materials* **2** 034010 ISSN 2053-1583 URL http://dx.doi.org/10.1088/2053-1583/2/3/034010

[41] Dai S, Xiang Y and Srolovitz D J 2016 *Phys. Rev. B* **93**(8) 085410 URL http://link.aps.org/doi/10.1103/PhysRevB.93.085410

[42] Dai S, Xiang Y and Srolovitz D J 2016 *Nano Letters* **16** 5923–5927

[43] Kolmogorov A N and Crespi V H 2005 *Phys. Rev. B* **71** ISSN 1550-235X URL http://dx.doi.org/10.1103/PhysRevB.71.235415

[44] Uchida K, Furuya S, Iwata J I and Oshiyama A 2014 *Phys. Rev. B* **90** 155451 ISSN 1550-235X URL http://dx.doi.org/10.1103/PhysRevB.90.155451

[45] Mostaani E, Drummond N D and Falko V I 2015 *Phys. Rev. Lett.* **115** 115501 ISSN 1079-7114 URL http://dx.doi.org/10.1103/PhysRevLett.115.115501

[46] Alden J S, Tsen A W, Huang P Y, Hovden R, Brown L, Park J, Muller D A and McEuen P L 2013 *Proceedings of the National Academy of Sciences* **110** 11256–11260 ISSN 1091-6490 URL http://dx.doi.org/10.1073/pnas.1309394110

[47] Jain S K, Juricic V and Barkema G T 2016 *Phys. Rev. B* **94** 020102(R) ISSN 2469-9969 URL http://dx.doi.org/10.1103/PhysRevB.94.020102

[48] Campanera J M, Savini G, Suarez-Martinez I and Heggie M I 2007 *Phys. Rev. B* **75** 235449 ISSN 1550-235X URL http://dx.doi.org/10.1103/PhysRevB.75.235449